Electron waves in chemically substituted graphene

N. M. R. Peres[1], F. D. Klironomos[2], S.-W. Tsai[2], J. R. Santos [1], J. M. B. Lopes dos Santos[3], and A. H. Castro Neto[4]
[1]*Center of Physics and Departamento de Física, Universidade do Minho, P-4710-057, Braga, Portugal*
[2]*Department of Physics and Astronomy, University of California, Riverside, CA 92521, USA*
[3]*CFP and Departamento de Física, Faculdade de Ciências Universidade de Porto, 4169-007 Porto, Portugal and*
[4]*Department of Physics, Boston University, 590 Commonwealth Avenue, Boston, MA 02215,USA*
(Dated: August 26, 2018)

We present exact analytical and numerical results for the electronic spectra and the Friedel oscillations around a substitutional impurity atom in a graphene lattice. A chemical dopant in graphene introduces changes in the on-site potential as well as in the hopping amplitude. We employ a T-matrix formalism and find that disorder in the hopping introduces additional interference terms around the impurity that can be understood in terms of bound, semi-bound, and unbound processes for the Dirac electrons. These interference effects can be detected by scanning tunneling microscopy.

PACS numbers: 73.20.Hb,81.05.Uw,73.20.-r, 73.23.-b

Introduction. Graphene [1], a one atom-thick layer of graphite, has been intensively studied [2, 3, 4, 5, 6, 7, 8, 9, 10, 11, 12] due to its fascinating physical properties [8, 9, 10]. Graphene is a zero-gap semiconductor and its low-energy electronic excitations are described in terms of a Dirac spectrum. Because of this, disorder in the form of impurities [8, 11, 12, 13, 14], defects [15, 16, 17, 18] and surfaces [19, 20] can have a strong effect, especially when the chemical potential crosses the Dirac point. In this work, we consider dilute chemical dopants in graphene incorporated as substitutional atoms, and calculate local single particle properties such as the electronic energy spectra, local density of states, and electron density distribution, which shows Friedel oscillations as depicted in Fig. (1). The results presented here can be measured by scanning tunneling microscopy (STM) [21, 22, 23].

Atomic substitution in a carbon (C) honeycomb lattice is chemically possible for boron (B) and nitrogen (N) atoms. There have been several experimental studies of B and N substitution in highly-oriented pyrolytic graphite (HOPG) [24, 25], graphitic structures [26], nanoribbons [27], carbon nanotubes [26, 28, 29, 30, 31, 32, 33, 34, 35, 36, 37] and fullerenes [38]. When B or/and N atoms replace a carbon atom in a graphene sheet they have the following effects: (1) they act as impurity scattering centers; (2) they act as hole- or electron-dopants; (3) they introduce lattice distortions. In the case of B there is an increase of the absolute value of the hopping amplitude given its larger atomic radius ($r \simeq 0.85$Å) as compared to C ($r \simeq 0.7$Å). On the other hand, a N atom impurity ($r \simeq 0.65$Å) can be modeled by a smaller hopping integral. For the change in the on-site energy, we assume the C on-site energy to be zero (our reference state); the smaller atomic number of B leads to a positive local energy, whereas on a site occupied by N, the local energy should be smaller and therefore is modeled as a negative local energy. The effect of a different on-site energy has been extensively studied in the past [8, 11, 12, 13, 14], but the effect on the hopping has been overlooked. In this work we study the combined effect of local changes in the atomic energy as well as the hopping amplitudes. A vacancy has been modeled by an infinite, on-site energy potential, but it is also exactly represented by the remotion of particular hopping processes from the Hamiltonian. The opposite limit of very large hopping to the impurity site corresponds to a four-atom molecule.

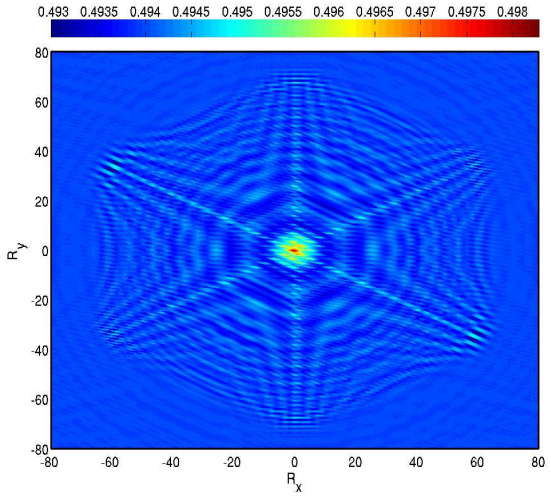

FIG. 1: (color on line) Real-space electronic distribution and Friedel oscillations around an impurity with ionic radius smaller than carbon (such as N) ($t_0 = 0.5t$).

Hopping and potential disorder. The honeycomb lattice has a unit cell represented in Fig. (2) by the vectors $\boldsymbol{a}_1$ and $\boldsymbol{a}_2$, such that $|\boldsymbol{a}_1| = |\boldsymbol{a}_2| = a$ ($a = \sqrt{3}a_0 \simeq 2.461$ Å, where a_0 is the carbon-carbon distance). In this basis any lattice vector $\boldsymbol{r}$ is represented as $\boldsymbol{r} = n\boldsymbol{a}_1 + m\boldsymbol{a}_2$, with n, m integers. In Cartesian coordinates, $\boldsymbol{a}_1 = a_0(3, \sqrt{3}, 0)/2$ and $\boldsymbol{a}_2 = a_0(3, -\sqrt{3}, 0)/2$. The reciprocal lattice vectors are given by: $\boldsymbol{b}_1 = 2\pi(1, \sqrt{3}, 0)/(3a_0)$ and $\boldsymbol{b}_2 = 2\pi(1, -\sqrt{3}, 0)/(3a_0)$, and the vectors connecting any A atom to its nearest neighbors are: $\boldsymbol{\delta}_1 = (\boldsymbol{a}_1 - 2\boldsymbol{a}_2)/3$, $\boldsymbol{\delta}_2 = (\boldsymbol{a}_2 - 2\boldsymbol{a}_1)/3$, and $\boldsymbol{\delta}_3 = (\boldsymbol{a}_1 + \boldsymbol{a}_2)/3$. Using these definitions the Hamiltonian can be written as: $H = H_0 + V_t + V_0$, where $H_0 = -t\sum_{\boldsymbol{r}}[b^\dagger(\boldsymbol{r})a(\boldsymbol{r}) + b^\dagger(\boldsymbol{r} - \boldsymbol{a}_2)a(\boldsymbol{r}) + b^\dagger(\boldsymbol{r} - \boldsymbol{a}_1)a(\boldsymbol{r}) + \text{h.c.}]$,

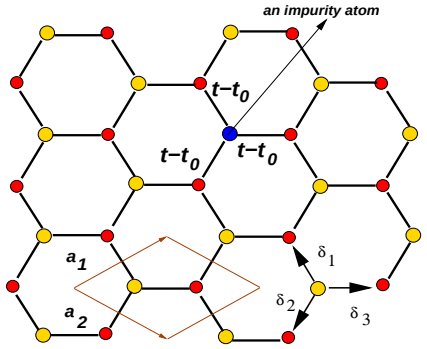

FIG. 2: (color on line) The honeycomb lattice with a carbon atom replaced by an impurity atom, such a B or N. The local hopping parameter changes from t to $t - t_0$.

is the kinetic energy operator and $a^\dagger$ ($b^\dagger$) are creation operators in the A (B) sites. The operators $V_t = t_0[b^\dagger(0)a(0) + b^\dagger(-\boldsymbol{a}_2)a(0) + b^\dagger(-\boldsymbol{a}_1)a(0) + \text{h.c.}]$ and $V_0 = \varepsilon_0 a^\dagger(0)a(0)$ are the impurity terms for hopping and potential disorder, respectively. In the particular case $t_0 = t$, the scattering term V_t represents a vacancy. In this work we consider the case of zero chemical potential when the Fermi level crosses the Dirac point. This is the case in which the system is most susceptible to the presence of impurities. The equations of motion for the Green's functions can be readily written, and are given by:

$$i\omega_n G_{aa}(\omega_n,\boldsymbol{k},\boldsymbol{p}) = \delta_{\boldsymbol{k},\boldsymbol{p}} + \sum_{\boldsymbol{q}} \left[\lambda_{\boldsymbol{k},\boldsymbol{q}} G_{ba}(\omega_n,\boldsymbol{q},\boldsymbol{p}) + \frac{\varepsilon_0}{N_c} G_{aa}(\omega_n,\boldsymbol{q},\boldsymbol{p}) \right]$$

$$i\omega_n G_{ba}(\omega_n,\boldsymbol{k},\boldsymbol{p}) = \sum_{\boldsymbol{q}} \lambda^*_{\boldsymbol{q},\boldsymbol{k}} G_{aa}(\omega_n,\boldsymbol{q},\boldsymbol{p})$$

$$i\omega_n G_{ab}(\omega_n,\boldsymbol{k},\boldsymbol{p}) = \sum_{\boldsymbol{q}} \left[\lambda_{\boldsymbol{k},\boldsymbol{q}} G_{bb}(\omega_n,\boldsymbol{q},\boldsymbol{p}) + \frac{\varepsilon_0}{N_c} G_{ab}(\omega_n,\boldsymbol{q},\boldsymbol{p}) \right]$$

$$i\omega_n G_{bb}(\omega_n,\boldsymbol{k},\boldsymbol{p}) = \delta_{\boldsymbol{k},\boldsymbol{p}} + \sum_{\boldsymbol{q}} \lambda^*_{\boldsymbol{q},\boldsymbol{k}} G_{ab}(\omega_n,\boldsymbol{q},\boldsymbol{p}) \,,$$

where $\lambda_{\boldsymbol{k},\boldsymbol{p}} = -t\phi_{\boldsymbol{p}}(\delta_{\boldsymbol{k},\boldsymbol{p}} - t_0/N_c t)$, $\phi_{\boldsymbol{p}} = 1 + e^{-i\boldsymbol{p}\cdot\boldsymbol{a}_1} + e^{-i\boldsymbol{p}\cdot\boldsymbol{a}_2}$, and N_c is the total number of unit cells in the lattice. The sublattice symmetry is broken by the presence of the impurity and this is manifested in the fact that $\lambda_{\boldsymbol{pq}} \neq \lambda_{\boldsymbol{qp}}$ and in the asymmetric way in which the ε_0-term appears in the equations above. The above set of equations can be solved exactly. The fact that the scattering term V_t depends on $\phi_{\boldsymbol{k}}$ leads to a more complex form for the T-matrix than usual. The exact solution for the Green's functions can be written in the form:

$$G_{aa}(\boldsymbol{k},\boldsymbol{p}) = \delta_{\boldsymbol{k},\boldsymbol{p}} G^0_{\boldsymbol{k}} + g + h\left[G^0_{\boldsymbol{k}} + G^0_{\boldsymbol{p}}\right] + G^0_{\boldsymbol{k}} T G^0_{\boldsymbol{p}} \,, \quad (1)$$

$$G_{bb}(\boldsymbol{k},\boldsymbol{p}) = \delta_{\boldsymbol{k},\boldsymbol{p}} G^0_{\boldsymbol{k}} + \frac{t\phi^*_{\boldsymbol{k}}}{i\omega_n} G^0_{\boldsymbol{k}} T G^0_{\boldsymbol{p}} \frac{t\phi_{\boldsymbol{p}}}{i\omega_n} \,. \quad (2)$$

where all the terms also depend on ω_n (omitted here for brevity). They are defined as:

$$g(\omega_n) = t_0^2 \bar{G}^0(\omega_n)/[N_c D(\omega_n)], \quad (3)$$

$$h(\omega_n) = t_0(t - t_0)/[N_c D(\omega_n)], \quad (4)$$

and

$$T(\omega_n) = -\frac{i\omega_n t_0(2t - t_0) - \varepsilon_0 t^2}{N_c D(\omega_n)} \quad (5)$$

where the denominator $D(\omega_n)$ is given by

$$D(\omega_n) = (t - t_0)^2 + \left[i\omega_n t_0(2t - t_0) - \varepsilon_0 t^2\right] \bar{G}^0(\omega_n) \quad (6)$$

and $\bar{G}^0(\omega_n) = \sum_{\boldsymbol{k}} G^0(\omega_n,\boldsymbol{k})/N_c$ with $G^0_{\boldsymbol{k}} = G^0(\omega_n,\boldsymbol{k}) = (i\omega_n)/[(i\omega_n)^2 - t^2|\phi_{\boldsymbol{k}}|^2]$, the diagonal Green's function for the clean system.

The significance of the term $g(\omega_n)$ in (1) which only appears in G_{aa}, is easily appreciated if we do the double Fourier transform to real space. This term only contributes to $G_{aa}(0,0)$, the return amplitude to the impurity site. The factor $1/D(\omega_n)$ contains a sum over an infinite series of intermediate scattering events, but the overall process is bounded and the t_0^2 factor denotes hopping from the impurity to the nearest neighbor B-sites and back to the impurity site. A similar interpretation can be given to another term which only appears in G_{aa}, namely, $G^0(\omega_n,k)h(\omega_n)$: this term contributes only to $G_{aa}(r,0)$ and describes an additional amplitude of propagation between the impurity site and another A site. No such terms can, of course, appear in G_{bb} when the inpurity is at an A site.

The exact general solution for both diagonal components of the Green's functions for a substitutional impurity with potential and hopping disorder is contained in (1) and (2) . The local density of states (LDOS) can be obtained from the Green's functions (1,2), after analytical continuation $i\omega_n \to \omega + i0^+$. For sites in the A and B sublattices, it is given by: $\rho_\nu(\boldsymbol{r},\omega) = -\text{Im}G_{\nu\nu}(\omega,\boldsymbol{r},\boldsymbol{r})/\pi$, where $\nu = a, b$ and $\boldsymbol{r}$ is the position of the unit cell. The local number of electrons, for a half-filled band, is obtained by:

$$n_{a,b}(\boldsymbol{r}) = \int_{-W}^{0} d\omega \rho_{a,b}(\boldsymbol{r},\omega) \,, \quad (7)$$

where $W = 3t$ is half of the total electronic bandwidth.

Strong suppression of hopping and vacancies. A vacancy corresponds to $t_0 = t$, leading to a simplified form for G_{aa}:

$$G_{aa}(\boldsymbol{k},\boldsymbol{p}) = G^0_{\boldsymbol{k}}\delta_{\boldsymbol{k},\boldsymbol{p}} + \frac{1}{N_c i\omega_n} - \frac{G^0_{\boldsymbol{k}}[\bar{G}^0]^{-1} G^0_{\boldsymbol{p}}}{N_c} \,, \quad (8)$$

where G_{aa}, G^0 and $\bar{G}^0$ also depend on ω_n, and the on-site impurity potential was set to zero ($\varepsilon_0 = 0$). Because the vacancy creates a three-site zig-zag edge, one expects the appearance of zero energy modes [8]. The $1/i\omega_n$ term in (8) leads to a contribution, $\rho_a(0,\omega) \propto \delta(\omega)$ in the total DOS, as shown in Fig. (3). This contribution comes from the atom that has been disconnected from the rest of the lattice. It corresponds to exactly one state and to properly represent a missing atom this contribution to the DOS should be ignored. At small energies ($\omega \ll t$) we obtain for the nearest neighbor B-sites that $G_{bb}(0,0,\omega) \approx -1/(9t^2\bar{G}^0(\omega))$, in agreement

with previous studies [8, 39, 40] for vacancy modeled as infinite on-site potential, $\varepsilon_0 = \infty$. In this limit, $\rho_b(0,\omega) \simeq (\sqrt{3}|\omega|/6\pi t^2)\{1+(36\pi^2/27)[\omega \ln|\sqrt{3}\omega^2/6\pi t^2|]^{-2}\}$ giving a resonance at $\omega = 0$. The full numerical calculation for all energies is shown in Fig. (3) for the impurity site and in Fig. (4) for the nearest neighbor sites, with the spatial dependence of the amplitude of the low-energy states shown in the insets.

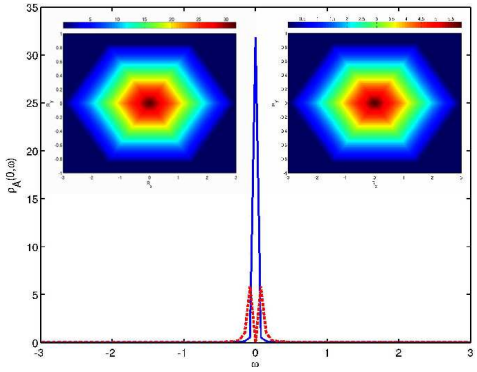

FIG. 3: (Color online) LDOS for $t_0 = t$ and $t_0 = 0.9t$ at the impurity site. Main graph corresponds to $\rho_a(0,\omega)$ for $t_0 = t$ (straight blue line) and for $t_0 = 0.9t$ (dashed red line). Left inset: $\rho_a(\boldsymbol{r},\omega = 0)$ for $t_0 = t$. Right inset: $\rho_a(\boldsymbol{r},\omega = -0.075t)$ for $t_0 = 0.9t$. Notice the scale difference.

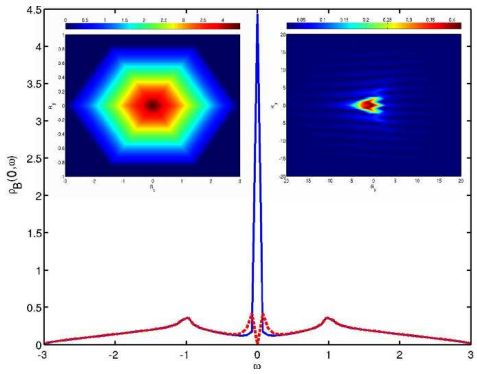

FIG. 4: (Color online) LDOS for $t_0 = t$ and $t_0 = 0.9t$ at the nearest neighbor sites of the impurity. Main graph corresponds to $\rho_b(0,\omega)$ for $t_0 = t$ (straight blue line) and for $t_0 = 0.9t$ (dashed red line). Left inset: $\rho_b(\boldsymbol{r},\omega = 0)$ for $t_0 = t$. Right inset: $\rho_b(\boldsymbol{r},\omega = -0.075t)$ for $t_0 = 0.9t$.

For t_0 slightly smaller than t, hopping to the impurity site is strongly suppressed but not completely absent. Hybridization between the low energy states at the impurity site and at the nearest neighbors sites leads to splitting into two resonant states, one with energy shifted to a negative value and the other to a positive value, as shown in Figs. (3-4).

Nitrogen substitution. As discussed previously, a N atom has a smaller atomic radius than a carbon atom, and this corresponds to a smaller hopping amplitude between the N impurity and the neighboring carbon atoms. In addition, the larger atomic number of N atoms gives a negative on-site potential ε_0 with respect to the carbon sites.

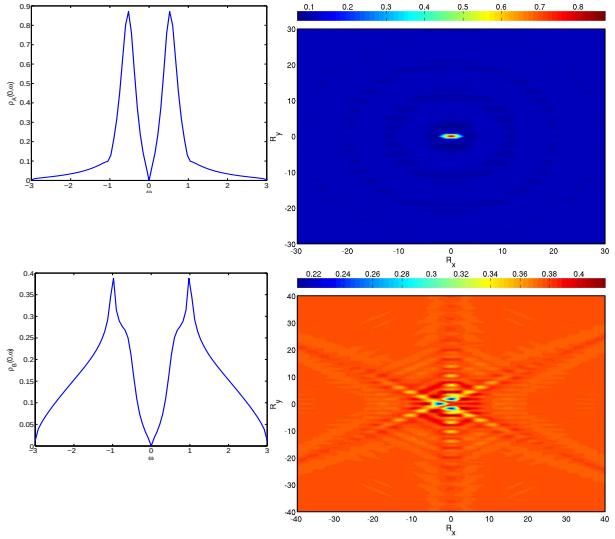

FIG. 5: (color on line) Left: LDOS at the impurity site (above) and at its nearest neighbors (below), for $t_0 = 0.5t$. Right: intensity plots of $\rho_a(\boldsymbol{r},\omega = -0.525t)$ (top), and $\rho_b(\boldsymbol{r},\omega = -0.975t)$ (bottom).

We first study the effects of hopping disorder alone, and consider the case $t_0 = 0.5t$. Fig. (1) shows an intensity plot of the real-space distribution of the number of electrons, given by (7). Interference effects give rise to Friedel oscillations displaying the underlying six-fold symmetry. The main contributions in the sum over negative states (7) come from: (i) the resonance states created by the impurity; and (ii) the spectral weight under the van Hove singularity that is also affected by the impurity. Fig. (5) shows these two contributions separately. In the left, we show the LDOS spectrum at the impurity site, and at its nearest-neighbors (B-sites). The spectrum shows a resonance peak at $\omega_0 = \pm 0.525t$ on the impurity, while for its nearest-neighbors it is mostly dominated by the van Hove peaks at $\omega \approx \pm t$ ($\omega_0 = \pm 0.975t$). The size of these peaks decreases away from the impurity and Fig. (5) shows the intensity plots of these peaks in real-space, which can be directly measured using STM spectroscopy.

When a negative ε_0 is also added, the LDOS gets modified as shown in Fig. (6) for the impurity and nearest neighbor sites. Any finite potential value at the impurity breaks particle-hole symmetry and as a result the spectrum becomes asymmetric under reflection ($\omega \to -\omega$).

Boron substitution. In this case the impurity site has larger hopping amplitude and a positive on-site potential. Fig. (7) shows the LDOS at the impurity and the nearest neighbor sites for a case with $t_0 = -0.5t$ (so that the hopping amplitude to the impurity, $t - t_0$, is larger than the homogeneous system) and $\varepsilon_0 = 0.525t$. The peaks of the LDOS at certain energies originate from impurity resonance states and van Hove singularities. The real-space intensity plots are at resonance: $\omega_0 = -2.935t$ for the sublattice-A LDOS, and $\omega_0 = -0.975t$

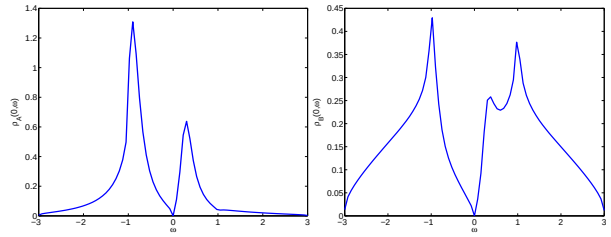

FIG. 6: LDOS for the case $t_0 = 0.5t$ and $\varepsilon_0 = -0.525t$, at the impurity site (left) and at the nearest neighbor sites (right).

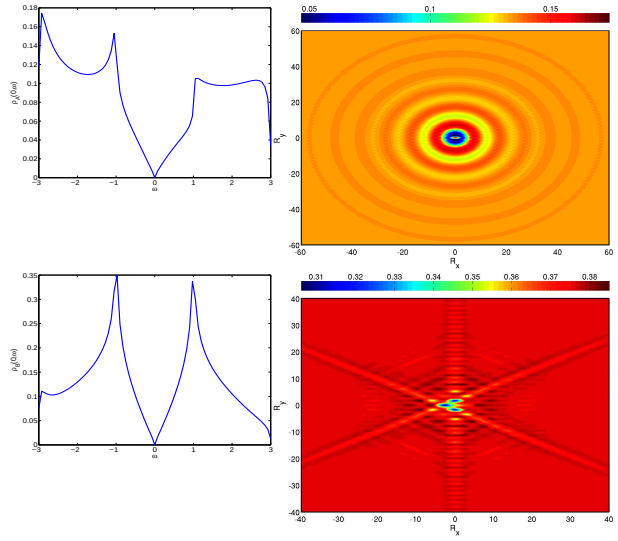

FIG. 7: (color on line) Electronic spectra for the case $t_0 = -0.5t$ and $\varepsilon_0 = 0.525t$, corresponding to an impurity such as boron. Left: LDOS at the impurity site (top) and nearest neighbors (bottom). Right: real-space intensity plot of $\rho_a(\boldsymbol{r}, \omega = -2.935t)$ (top), and $\rho_b(\boldsymbol{r}, \omega = -0.975t)$ (bottom).

(at the van Hove singularity) for the sublattice-B LDOS. Just as for the case of N shown in Fig. (5) the van Hove singularities are more strongly affected at certain directions. The van Hove peaks are strongest on B-sites where the LDOS can be understood as being originated by three impurities (the three nearest neighbor B-sites of the actual impurity site) and hence the star-shaped symmetry shown in the intensity maps at $\omega_0 = -0.975t$ in Fig. (5) and Fig. (7). Near the band edge, the band structure of the clean system behave more like a conventional 2D system, so the resonance peak at $\omega_0 = -2.935t$ has a symmetric spatial distribution (Fig. (7), top).

Conclusions. We find the exact electronic Green's functions in the presence of an impurity that modifies both the local atomic energy as well as the hopping amplitude with neighboring C atoms. We have shown that the presence of the impurity leads to strong modifications of the local density of states and also to the presence of unusual Friedel oscillations, both quantities being accessible to measurement through STM spectroscopy. We have applied our theory to the case of substitutional B and N and found that these two atoms have very specific spectroscopic signatures. From the knowledge of these Green's function one can also calculate the transport properties of chemically substituted graphene.

We thank the hospitality of the KITP at UCSB, (NSF grant No. PHY05-51164), where part of this work was performed. We thank A. D. Klironomos and V. M. Pereira for useful discussions. JMBLS and NMRP acknowledge financial support from POCI 2010 via project PTDC/FIS/64404/2006. A.H.C.N. was supported through NSF grant DMR-0343790.

[1] K. S. Novoselov, *et al.*, Science **306**, 666 (2004).
[2] K. S. Novoselov, *et al.*, Proc. Nat. Acad. Sc. **102**, 10451 (2005).
[3] K. S. Novoselov, *et al.*, Nature **438**, 197 (2005).
[4] Y. Zhang, *et al*, Phys. Rev. Lett. **94**, 176803 (2005).
[5] Y. Zhang, *et al.* Appl. Phys. Lett. **86**, 073104 (2005).
[6] Y. Zhang, *et al.* Nature **438**, 201 (2005).
[7] C. Berger, *et al.*, J. Phys. Chem. B **108**, 19912 (2004)
[8] N. M. R. Peres, F. Guinea, and A. H. Castro Neto, Phys. Rev. B **73**, 125411 (2006).
[9] A. H. Castro Neto, F. Guinea, and N. M. R. Peres, Phys. World **19**, 33 (2006).
[10] A. K. Geim and K.S. Novoselov, Nature Mat. **6**, 183 (2007).
[11] V. M. Pereira, *et al.*, Phys. Rev. Lett. **96**, 036801 (2006).
[12] Yu. V. Skrypnyk and V. M. Loktev, Phys. Rev. B **73**, 241402 (2006).
[13] V. V. Cheianov and V. I. Falko, Phys. Rev. Lett. **97**, 226801 (2006).
[14] T. O. Wehling, *et al.* cond-mat/0609503.
[15] M. A. H. Vozmediano *et al.*, Phys. Rev. B **72**, 155121 (2005).
[16] A. Cortijo and M. A. H. Vozmediano, Nucl.Phys. **B763**, 293 (2007).
[17] O. V. Yazyev *et al.*, Phys. Rev. B **75**, 115418 (2007).
[18] O. V. Yazyev and L. Helm, Phys. Rev. B **75**, 125408 (2007).
[19] A. H. Castro Neto, F. Guinea, and N. M. R. Peres, Phys. Rev. B **73**, 205408 (2006).
[20] N. M. R. Peres, A. H. Castro Neto, and F. Guinea, Phys. Rev. B **73**, 195411 (2006).
[21] Y. Niimi, *et al.*, Phys. Rev. Lett. **97**, 236804 (2006).
[22] Y. Niimi, *et al.* Phys. Rev. B **73**, 085421 (2006).
[23] G. Li and E. Y. Andrei, arXiv:0705.1185 (2007).
[24] E. J. Mele and J. J. Ritsko, Phys. Rev. B **24**, 1000 (1981).
[25] M. Endo, *et al.*, J. Appl. Phys. **90**, 5670 (2001).
[26] O. Stephan, *et al.*, Science **266**, 1683 (1994).
[27] T. B. Martins *et al.*, Phys. Rev. Lett. **98**, 196803 (2007).
[28] M. Yudasaka *et al.*, Carbon **35**, 195 (1997).
[29] R. Sen, *et al.*, Chem. Phys. Lett. **287**, 671 (1998).
[30] M. Terrones, *et al.*, Appl. Phys. Lett. **75**, 3932 (1999).
[31] D. Golberg, *et al.*, Carbon **38**, 2017 (2000).
[32] W.-Q. Han, *et al.* App. Phys. Lett. **77**, 1807 (2000).
[33] R. Kurt, *et al.*, Carbon **39**, 2163 (2001).
[34] R. Kurt, *et al.*, Thin Solid Films **398-299**, 193 (2001).
[35] S. Trasobares, *et al.*, J. Chem. Phys. **116**, 8966 (2002).
[36] C. J. Lee, *et al.*, Chem. Phys. Lett. **359**, 115 (2002).
[37] M. Terrones, *et al.*, App. Phys. A **74**, 355 (2002).
[38] T. Guo, C. Jin, and R. E. Smalley, J. Phys. Chem. **95**, 4948 (1991).
[39] P. A. Lee, Phys. Rev. Lett. **71**, 1887 (1993).
[40] A. V. Balatsky, M. I. Salkola, and A. Rosengren, Phys. Rev. B **51**, 15547 (1995).